Hysteresis Compensator With Learning-Based Hybrid Joint Angle Estimation for Flexible Surgery Robots

Donghoon Baek, Ju-Hwan Seo, Joonhwan Kim, and Dong-Soo Kwon

***Abstract*—Hysteresis causes difficulties in precisely controlling motion of flexible surgery robots and degrades the surgical performance. In order to reduce hysteresis, model-based feed-forward and feedback-based methods using endoscopic cameras have been suggested. However, model-based methods show limited performance when the sheath configuration is deformed. Although feedback-based methods maintain their performance regardless of the changing sheath configuration, these methods are limited in practical situations where the surgical instruments are obscured by surgical debris, such as blood and tissues. In this letter, a hysteresis compensation method using learning-based hybrid joint angle estimation (LBHJAE) is proposed to address both of these situations. This hybrid method combines image-based joint angle estimation (IBJAE) and kinematic-based joint angle estimation (KBJAE) using a Kalman filter. The proposed method can estimate an actual joint angle of a surgical instrument as well as reduce its hysteresis both in the face of partial obscuration and in different sheath configurations. We use a flexible surgery robot, K-FLEX, to evaluate our approach. The results indicate that the proposed method has effective performance in reducing hysteresis.**

***Index Terms*—Surgical robotics: medical robots and systems, deep learning in robotics and automation, tendon/wire mechanism.**

I. Introduction

MANY different types of flexible endoscopic surgery robots have been developed for next-generation robotic surgery to overcome the limitations of rigid instruments and conventional endoscopes [1]. These robots can access lesions through a curved path, which cannot be achieved using a rigid instrument. Moreover, these systems provide dexterous motion using the multiple degrees of freedom (DOFs) of the surgical instruments to perform complex surgical tasks.

A common mechanism in these systems is the tendon-sheath mechanism (TSM). This offers several advantages in flexible surgery robot applications, such as efficient transmission, flexibility, and small size. However, the precise motion control of the surgical instruments using the TSM is a highly challenging issue because of hysteresis caused by nonlinear friction, backlash, and wire elongation and slackening [2]. This phenomenon greatly degrades the control accuracy of surgical instruments and limits the user's performance with the system.

Two different approaches have been attempted to reduce hysteresis in flexible surgical robots. Firstly, the hysteresis model-based method [3] and feed-forward control approaches have been suggested [4]. Additionally, Xu *et al.* [5] and Rafael *et al.* [6] suggested a data-driven method toward learning the inverse kinematics of TSM considering hysteresis. However, their performance may be degraded if *a priori* hysteresis characteristics are converted. Deformation of the sheath configuration is one of the major causes of changing hysteresis characteristics in actual operation.

Secondly, several feedback-based methods have been proposed. Reichl *et al.* used electromagnetic position sensors for the pose measurement of a surgical instrument [8]. However, these sensors cannot be mounted on surgical instruments because they cannot be sterilized and their size is prohibitive. Given the limitations of the aforementioned approaches, vision-based pose estimation algorithms for estimating the actual pose of surgical instruments using a camera are being actively studied [9]–[11]. Some of these have even been applied in *in-vivo* environments. However, unfortunately, a need remains for research to improve control performance for surgical robots using estimation methods. There are two ways to reduce the hysteresis of surgical instruments using vision feedback: one employs markers and the other does not. Reilink *et al.* suggested a compensation method with vision feedback using markers that can easily be covered with surgical debris [12]. Recently, the previous work of the authors proposed a hysteresis compensator using a learning-based method without using markers [13]. These are robust against changing hysteresis characteristics such as deformation of the sheath configuration, but inherently vulnerable to occlusion problems caused by surgical debris, such as blood, tissues, and surgical smoke.

Manuscript received September 10, 2019; accepted January 16, 2020. Date of publication February 10, 2020; date of current version September 9, 2020. This letter was recommended for publication by Associate Editor C. Rucker and Editor P. Valdastri upon evaluation of the reviewers' comments. This work was supported by the International Joint Technology Development Project funded by the Korean Ministry of Trade, Industry and Energy under Grant P0006718. *(Corresponding author: Dong-Soo Kwon.)*

Donghoon Baek is with the Robotics Program, Korea Advanced Institute of Science and Technology, Daejeon, South Korea, and also with the researcher of EasyEndo Surgical Inc. (e-mail: romansabaek@kaist.ac.kr).

Ju-Hwan Seo and Joonhwan Kim are with the Department of Mechanical Engineering, Korea Advanced Institute of Science and Technology, Daejeon, South Korea (e-mail: seojh1989@kaist.ac.kr; joonhwan@kaist.ac.kr).

Dong-Soo Kwon is with the Department of Mechanical Engineering, Korea Advanced Institute of Science and Technology, Daejeon, South Korea, and also with the CEO of EasyEndo Surgical Inc. (e-mail: kwonds@kaist.ac.kr).

This letter has supplementary downloadable material available at https://ieeexplore.ieee.org, provided by the authors.

Digital Object Identifier 10.1109/LRA.2020.2972821

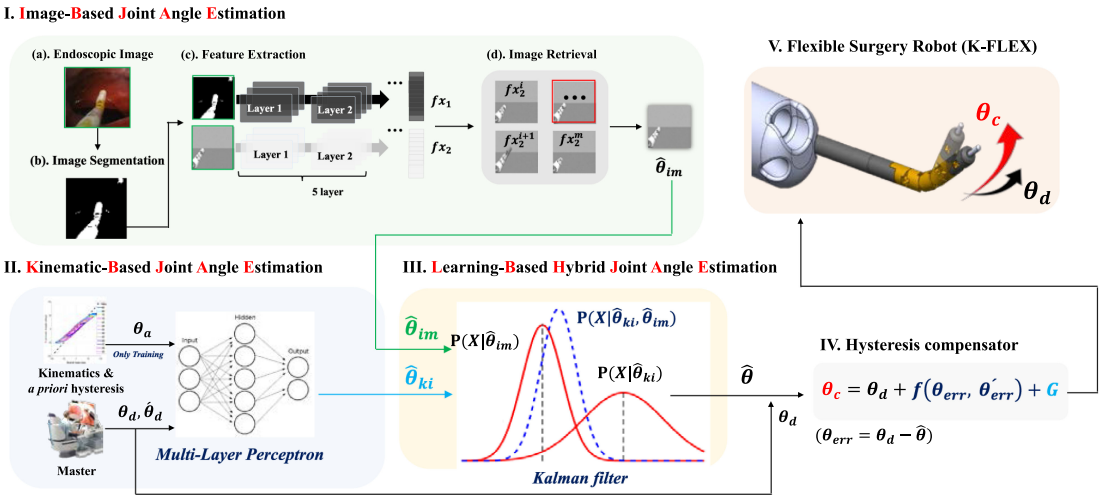

Fig. 1. Steps of proposed hysteresis compensation process. I. Estimation of actual joint angle using IBJAE. II. Estimation of actual joint angle using KBJAE. III. LBHJAE, combination algorithm of IBJAE and KBJAE using Kalman filter. IV. Hysteresis compensator. V. Target surgical instrument.

In this letter, we propose a hysteresis compensation method that can reduce the hysteresis of surgical instruments despite their being partially obscured even considering deformation of the sheath configuration. The proposed method utilizes learning-based hybrid joint angle estimation (LBHJAE), which incorporates image-based joint angle estimation (IBJAE) and kinematic-based joint angle estimation (KBJAE) using a Kalman filter. IBJAE predicts the joint angle using a Siamese convolutional neural network (SCNN) to extract features [15] in the 2D appearance of the instrument on the image. KBJAE also estimates the joint angle by using a multilayer perceptron (MLP) which employs kinematics and *a priori* hysteresis as features for learning. Both methods work complementarily, improving hysteresis reduction performance in situations where the instrument is obscured or the sheath configuration is changed. Moreover, we showed that our method is effective in reducing hysteresis in a real flexible surgical robot system as well.

II. Materials and Methods

The process of the proposed method consists of five major parts (see Fig. 1). KBJAE and IBJAE both estimate the joint angles and these are fused by the Kalman filter. The final estimated joint angle obtained from LBHJAE is utilized for the feedback compensator, which compensates for the position command. In this work, our aim is to reduce the hysteresis of the surgical instrument bending joint which is uniquely driven by the TSM and most affected by hysteresis. Several research studies have also focused on reducing the hysteresis of the bending joint [4], [7]. Moreover, Kim *et al.* have shown that reducing the bending joint backlash hysteresis of the surgical tool results in improved surgical performance [14]. Moreover, we have assumed that the camera is stationary, taking into account its application as a flexible surgery robot [1].

A. Targeted Flexible Endoscopic Surgery Robot System

A typical form of flexible endoscopic surgery robot was used as a target system. This has a surgical instrument, an endoscopic camera, and a distal part of the overtube, as shown in Fig. 2(a). The surgical instrument is constructed by a hyper-redundant continuum joint, and two DOFs (translation d, bending θ) are used in this work. The surgical instrument is driven by a TSM for its bending motion as shown in Fig. 2(b). The inverse kinematic model between a variation of wire length ΔL and joint angle θ is given as follows:

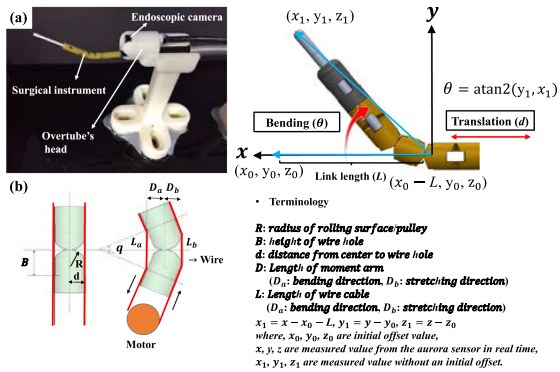

Fig. 2. (a) Target flexible endoscopic surgery robot system. (b) TSM in target system.

$$\Delta L_a(\theta) = 2n\left\{R - d\sin\left(\frac{\theta}{2n}\right) - (R-B)\cos\left(\frac{\theta}{2n}\right) - B\right\} \tag{1}$$

$$\Delta L_b(\theta) = \Delta L_a(-\theta) \tag{2}$$

where n is the number of segments constituting a continuum joint ($n = 2$), and the other terminologies are described in Fig. 2. This kinematic model was used for the control of the TSM.

B. Hysteresis Compensator

The concept of the hysteresis compensator involves providing an additional position input, and its control flow is shown in Fig. 3. The structure of the compensator was based on the PID

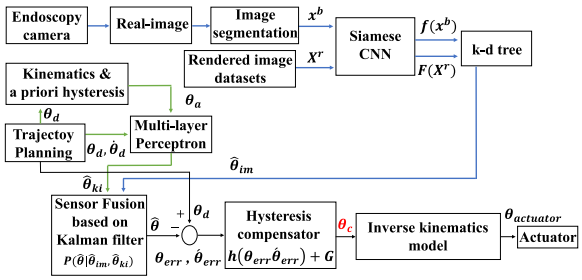

Fig. 3. Control diagram of proposed hysteresis compensation method.

controller, and it can be expressed as follows:

$$\theta_c = \theta_d + f\left(\theta_{err}, \theta'_{err}\right) + G \tag{3}$$

$$f\left(\theta_{err}, \theta'_{err}\right) = K_p\theta_{err} + K_d\theta'_{err} + K_i \int \theta_{err} dt \tag{4}$$

where the position error θ_{err} is $\theta_{err} = \theta_d - \hat{\theta}$, θ_d is the desired angle from the master controller, and $\hat{\theta}$ is an estimated angle from LBHJAE. Parameters θ_c and θ'_{err} denote the compensated position input and the differential of θ_{err}, respectively. K_p, K_d, and K_i are the hyperparameters for the proposed compensator. G is the backlash compensation term defined as follows:

$$G_t = -f(\theta_{err}, \theta'_{err})_{t-1} \tag{5}$$

where t is a time step. Therefore, the opposite value is compensated at the previous time. G_t is only updated when the direction of the input command changes.

C. Learning-Based Hybrid Joint Angle Estimation

The proposed LBHJAE is a fusion method combining IBJAE and KBJAE using a Kalman filter. Both act as sensors for measurement updates in a Kalman filter. IBJAE can estimate the pose of surgical instruments regardless of sheath configurations. KBJAE can estimate the pose of the instruments when surgical instruments are occluded. Therefore, they can complement each other for each case.

1) Image-Based Joint Angle Estimation (IBJAE): The concept of IBJAE is image retrieval (i.e., searching for the most similar image in a large database). IBJAE consists of the following procedures (see Fig. 4): (1) segmenting the image for splitting the clinical background and the surgical instrument; (2) extracting the features $\{f_{x1}, f_{x2}\}$ that determine a "similarity" indicating whether the two images $\{x^b, x^r\}$ are in the same category; and (3) searching for the most similar image in a pre-built database.

To remove the effect of the clinical background for extracting features from the surgical tool image efficiently, a region-based segmentation approach was applied. This includes functions such as region of interest, split, merge, and threshold, as shown in Fig. 4(b) [16].

Because IBJAE uses a SCNN, which employs a unique structure to naturally rank the similarity between two images [16], we constructed a database $\mathcal{D}^I$ for training the SCNN, as shown in Fig. 4(a). We used an open source robot simulator Gazebo to gather a reliable image dataset with joint angle labels without physical noise. The database $\mathcal{D}^I$ contained data $D_i^I = \{S_i, X_i^b, X_i^r\}, D^I \in \mathcal{D}^I, i \in [1,\ 100,000]$ consisting pairs of images. One was a binary image, $X^b = \{x^b, d^b, \theta^b\}$, and the other was a rendered image, $X^r = \{x^r, d^r, \theta^r\}$ where x^b and x^r are image obtained from a surgical robot system and the simulator consisting of the 3D-CAD model of the surgical robot and virtual camera, respectively. Parameter d expresses a translation motion, and θ is an actual joint angle of the surgical instrument (see Fig. 2). The label $S = \{1, 0\}$ represents whether two images $\{x^b, x^r\}$ are similar. We assumed $S = 1$ whenever x^r and x^b were similar images and $S = 0$ otherwise. The range of θ ($0° < \theta < 50°$) was decided by considering ranges commonly used in surgery [17] and the camera's field of view. The ground truth joint angle θ was measured by using an electromagnetic position measurement sensor called Aurora (Northern Digital Inc, Canada). To reduce the effect of illumination noise, we made an additional dataset with Gaussian noise $x_w^b \sim \mathcal{N}(0, 0.01)$ as a data augmentation technique.

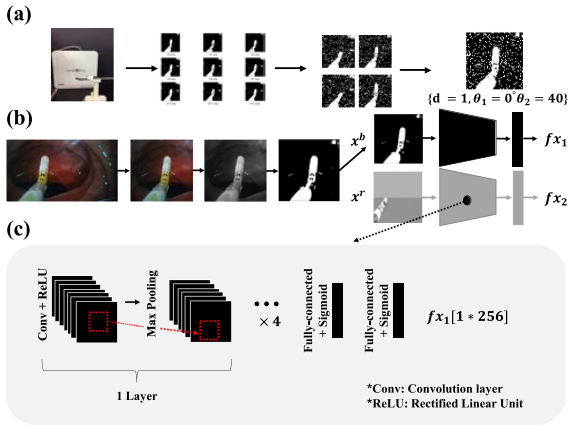

Fig. 4. (a) Database construction. (b) Process of region-based image segmentation and concept of SCNN. (c) Structure of SCNN.

TABLE I
CONFIGURATION OF THE SCNN

Layer name	Layer composition
Conv1	Conv2(32,5,1,0) + ReLU Max pooling (3,2,0)
Conv2	Conv2(64,3,1,0) + ReLU Max pooling (3,2,0)
Conv3	Conv2(128,3,1,0) + ReLU Max pooling (3,2,0)
Conv4	Conv2(256,3,1,0) + ReLU Max pooling (3,2,0)
Conv5	Conv2(256,3,1,0) + ReLU Max pooling (3,2,0)
FC (1)	Fully connected (1×256) + Sigmoid
FC (2)	Fully connected (1×256) + Sigmoid

A SCNN has two branches sharing the same architectures and weight values. The structure of the SCNN used in this work is modified from a recent letter using SCNN that takes a binary image as input [26]. The architecture of SCNN is described in Fig. 3(c) and summarized in Table I. Conv2(*k, n, s, p*) indicates a convolutional layer, where *k* is the filter size, *n* is the number of filters, *s* is a stride parameter, and *p* is a padding parameter. These parameters retained the same meaning in the Max pooling.

FC-256 denotes a fully connected layer that has 256 nodes. The rectified linear unit (ReLU) was used for an activation function. At the end of the network, the contrastive loss function *L* was used to learn a feature space that narrowed the distance between two similar images and widened the distance between two different images. In addition, we adopted a regularization technique for our loss function *L* to prevent overfitting. The L2 norm was used to express the distance between two images.

We used the Adam optimizer [18] for training the network with a batch size of 200. The size of the input image was 48 $\times$ 48 and the initial learning rate was $1e^{-4}$ with a 0.96 learning rate decay per epoch. The Xavier initialization [19] was used for initializing the weights of the network.

The k-d tree, an efficient searching method was used to determine the most similar image rapidly through a comparison with the feature vectors F_{x2} ($f_{x2} \in F_{x2}$) that the rendered images X^rwere pre-converted to by using the trained SCNN model. Each f_{x2} was labeled with the actual position {*d,* θ} of the surgical instrument. Thus, the joint angle θ of the surgical instrument could be estimated when the most similar image was obtained.

2) Kinematic-Based Joint Angle Estimation (KBJAE): The objective of KBJAE is to estimate the joint angle θ with the input $\{\theta_d,\ \theta'_d\}$ from the master controller, where θ_d is a position input, and θ'_d is an angular velocity. A multilayer perceptron (MLP), a kind of artificial neural network (ANN) was employed. The motivation for using two parameters $\{\theta_d,\ \theta'_d\}$ as features for learning came from the classic Bouc Wen model which uses the parameters for predicting hysteresis [20]. Because of hysteresis, θ can be described as follows:$\theta = \theta_d + \tilde{\theta}$, where $\tilde{\theta}$ is a position error from hysteresis induced by various physical factors. We expect that if $\tilde{\theta}$ can be estimated, an actual joint angle θ can also be predicted. To estimate $\widetilde{\theta}$, we designed the estimator E_w, where *w* is a parameter to be optimized. The objective function *C* is defined as follows:

$$\min_w C = \sum_{i=1}^{N} \left(E_w \left(\theta_d^{(i)},\ \ \theta_d'^{(i)} \right) - \tilde{\theta}^{(i)} \right)^2 \tag{6}$$

where $\tilde{\theta}^{(i)} = \theta_a^{(i)} - \theta_d^{(i)}$ and *N* is the batch size of the data. Our task is to find the value of the parameter *w* that minimizes *C*.

We obtained the dataset $\mathcal{D}^k = \{D_1^k, \ldots, D_{12}^k\}$, where $D^k \in \mathcal{D}^k$, $D^k = \{\theta_d^{(i)},\ \ \theta_d'^{(i)},\ \ \theta_a^{(i)}\}_{i=1}^m, m = 50,000$ by running the instrument of the target surgical robot platform. Each D^k is constructed given several periodic signals with different magnitudes in a straight sheath configuration. The actual joint angle θ_a as the ground truth was obtained from the Aurora sensor.

The structure of the MLP is summarized in Table II. The MLP consisted of three hidden layers. This includes the leakyReLU as an activation function and dropout for preventing overfitting. This was trained by using an Adam optimizer with a batch size of 200. The learning parameters were $3e^{-5}$for the initial learning rate and, 0.95 for the learning rate decay per epoch. The weights of the network were initialized using the He initialization technique [21].

3) Learning-Based Hybrid Joint Angle Estimation (LBHJAE): LBHJAE is a fusion method that combines KBJAE and IBJAE. This concept is similar to multi-sensor data fusion, which is defined as the synergy of measurements from multiple sensors to produce a single unified sensor [22]. KBJAE and IBJAE are employed as sensors for estimating the joint angle θ.

TABLE II
STRUCTURE OF MLP

Layer name	Layer composition
Input layer	Input [2, 200]
Hidden layer 1	Fully connected [200, 200] + leakyReLU Dropout (0.7)
Hidden layer 2	Fully connected [200, 200] + leakyReLU Dropout (0.7)
Hidden layer 3	Fully connected [200, 200] + leakyReLU Dropout (0.7)
Output layer	Output [200, 1]

The Kalman filter, one of the most widely used techniques for sensor fusion, is utilized as a fusion method. A simple linear dynamic model that is commonly used for smoothing data is applied because the analytic kinematic model, which represents the transformation between θ and actuations, is inaccurate due to hysteresis and can even be converted unpredictably due to the varying sheath configuration. The linear model and measurement equations corresponding to sensor-1 (KBJAE), and sensor-2 (IBJAE) are defined as follows:

$$x_k = Fx_{k-1} + \mathrm{G}a_k \tag{7}$$

$$z_{1k} = H_1 x_k + \mathrm{v}_{1k}, \quad \mathrm{v}_{1k} \sim \mathcal{N}(0, R_1) \tag{8}$$

$$z_{2k} = H_2 x_{2k} + \mathrm{v}_{2k}, \quad \mathrm{v}_{2k} \sim \mathcal{N}(0, R_2) \tag{9}$$

Eq. (7) describes the linear model and we assume that uncontrolled forces cause a constant acceleration of $a_k, a_k \sim \mathcal{N}(0, \sigma_a)$ between the $(k-1)$ and *k* time steps. Therefore, Eq. (7) can be defined as follows:

$$x_k = Fx_{k-1} + \mathrm{w}_k \tag{10}$$

$$x_k = [\theta_k,\ \ \theta'_k\ ]^T, F = \begin{bmatrix} 1 & \Delta t \\ 0 & 1 \end{bmatrix}, \tag{11}$$

$$H_{1,2} = \begin{pmatrix} 1 & 0 \\ 0 & 0 \end{pmatrix}, \quad R_1 = \begin{pmatrix} \sigma_{1z}^2 & 0 \\ 0 & 1 \end{pmatrix}, \quad R_2 = \begin{pmatrix} \sigma_{2z}^2 & 0 \\ 0 & 1 \end{pmatrix} \tag{12}$$

where x_k is the system state, F is the system matrix, Δt is a sampling period ($\Delta t = 0.1$) and, $w_k \sim \mathcal{N}(0, \mathrm{Q})$where $\mathrm{Q} = GG^T\sigma_a^2$ ($\sigma_\mathrm{a} = 0.01$). The measurements z_{1k} and z_{2k} are obtained from KBJAE and IBJAE, respectively (i.e., $z_{1k,\ 2k} = [\theta_k,\ 0]^\mathrm{T}$). The measurement noises v_{1k} and v_{2k} are also normally distributed, with a zero mean and standard deviation σ_z.

The estimated joint angle $\hat{\theta}$ is predicted by the following process (see Fig. 5) Let $\hat{x}_k^-$ be the *a priori* estimate and $\hat{\mathrm{P}}_k^-$ be the *a priori* covariance matrix at time *k* which is defined as $\mathrm{P}_k = \mathrm{E}[e_k e_k^T]$, $e_k = x_k - \hat{x}_k$, and $P_0 = diag(0,\ 0)$, where $\hat{x}_0 = [0,\ 0]^T$. Here, K_{1k} and K_{2k} are the Kalman gain matrices updated by KBJAE and IBJAE at step *k*, respectively. The state covariance matrices P_{1k} and P_{2k} are also updated by each of the above methods. Q and $R_{1,2}$ are usually assumed to be constant during updating. In our case, σ_{1z} and σ_{2z} which decide the more

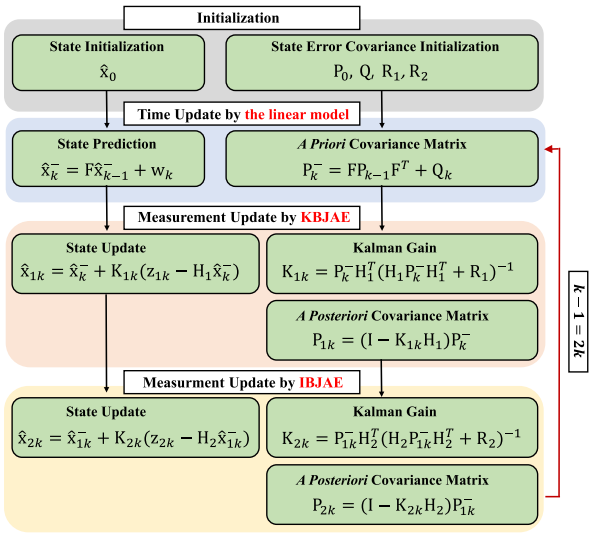

Fig. 5. Estimated bending angle update process using KBJAE and IBJAE.

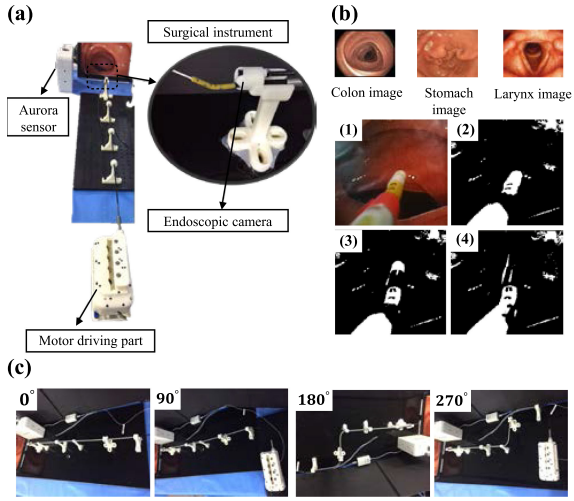

Fig. 6. Experiment setup. (a) Flexible surgery robot testbed. (b) Three different printed organ images and occlusion condition: (1) Instrument artificially covered by tape. (2) Occlusion 20%. (3) Occlusion 40%. (4) Occlusion 40% (distal part). (c) Different sheath configurations.

reliable one between IBJAE and KBJAE were chosen to be the same value ($\sigma_{1z},\ _{2z} = 0.01$). The estimated bending angle $\hat{\theta}$ is finally obtained.

III. Experimental Results

The experiments consist of three parts: (1) the evaluation of the generalizability of learning for each of the KBJAE and IBJAE models, (2) the evaluation of the joint angle estimation performance for LBHJAE, and (3) the evaluation of the bending joint hysteresis reduction performance for LBHJAE. Experiments (2) and (3) are performed taking into account occlusion and various sheath configuration conditions. In all experiments, Q, R_1 and R_2, which express reliability, are set to be the same value, as mentioned in Section II.

The flexible surgery robot testbed, manufactured using PAI materials that did not interfere with the sensing process, was used for a target system to validate the proposed method in both experiments, as shown in Fig. 6(a). Two DOFs (translation d and pitch θ) were operated to verify the feasibility of the proposed method. In this system, a micro USB endoscopic camera (MD-V31105L-77, MISUMI, Taiwan) with 1920 $\times$ 1080 resolution was mounted on the center of the overtube to take images. Three different printed clinical images {Colon, Stomach, Larynx} were used as the background for mimicking a real surgery environment as shown in Fig. 6(b). To measure an actual joint angle, the Aurora sensor was utilized. All system software was constructed on Linux (ubuntu18.04LTS) with ROS (melodic). The learning process was carried out using an NVIDIA RTX-2080ti GPU in a desktop.

A. Evaluation of Joint Angle Estimation Performance

1) Generalizability Performance Evaluation of KBJAE and IBJAE models: The purpose of the first experiment was to verify the generalizability performance of KBJAE and IBJAE. Generalizability is meaningful as an indicator to determine whether the deep learning model is overfitting the training data.

TABLE III
Generalizability Performance Results of KBJAE in Different Trajectory Inputs

	With a training dataset					
Amplitude	*35*	*45*	*55*	*65*	*75*	*85*
RMSE (°)	*1.65*	*1.67*	*1.22*	*1.60*	*1.46*	*1.90*
	With a test dataset					
Amplitude	*30*	*40*	*50*	*60*	*70*	*80*
RMSE (°)	*1.45*	*2.75*	*1.41*	*1.50*	*2.99*	*1.96*

TABLE IV
Generalizability Performance Results of IBJAE

	With a training dataset	*With a test dataset*
RMSE (°)	*0.147*	*1.57*

The root mean square error (RMSE) between the estimated $\hat{\theta}$ and the ground truth θ was used as an evaluation index. For KBJAE, showing generalizability for different positions and velocity signals is important. Therefore, we divided the dataset $\mathcal{D}^k$ into a training set and test set considering different signals that have different amplitudes and velocities. For IBJAE, we used 20% of the entire dataset $\mathcal{D}^I$ as a random test set.

The results for KBJAE can be seen in Table III. The average RMSE was 1.34° and 2.61° when using the training dataset and test dataset, respectively. The results for IBJAE are summarized in Table IV. When using the best model among the models we trained, RMSE was about 2° in both. Considering that the resolution of driving angles was1° in $\mathcal{D}^k$ and $\mathcal{D}^I$, the results are not significantly large.

2) Evaluation of Joint Angle Estimation Performance of LBHJAE: The proposed method (LBHJAE) was assessed to verify that it could estimate the actual joint angle of the surgical

TABLE V
ESTIMATION RESULTS WITH OBSCURED PART

		Percentage of obscured part			
Case		*0%*	*20%*	*40%*	*40% (Distal part)*
RMSE (°)	*KBJAE*	*2.37±0.27*	*2.92±0.24*	***2.73±0.9***	***3.13±0.35***
	IBJAE	*2.99±0.27*	*2.34±0.3*	*9.86±1.91*	*27.1±0.97*
	LBHJAE	***2.31±0.33***	***1.99±0.05***	*4.54±0.98*	*12.6±0.58*

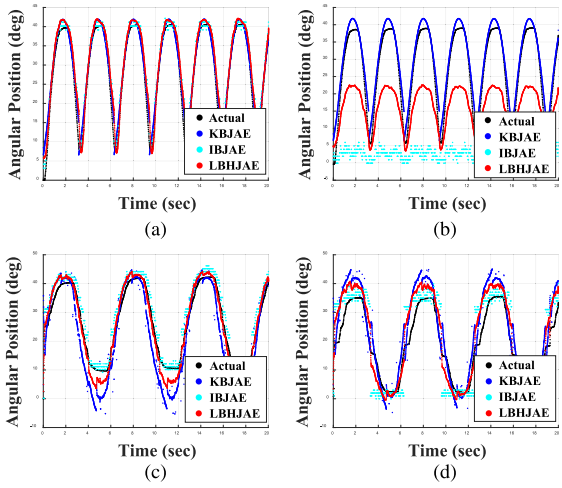

Fig. 7. Results of joint angle estimation. (a) No occlusion and configuration 0°. (b) 40% occlusion and configuration 0°. (c) No occlusion and configuration 270°. (d) 40% occlusion and configuration 270°. (Actual: black, KBJAE: blue, IBJAE: cyan, LBHJAE: red).

instrument when the instrument was partially obscured and the shape of the sheath was deformed.

To see the effects of occlusion, four different occlusion cases: 0%, 20%, 40%, and 40% (distal part) were used for the experiment (see Fig. 6(b)). These were determined based on the area covered by the tape. We attached red tape, similar to bloody surgical debris, to the surgical instrument. To evaluate the estimation performance as sheath configuration changed, four different sheath configurations {0°, 90°, 180°, 270°} were considered. This was selected in consideration of possible cases of surgery varying from the neck to the large intestine.

The results indicated that the estimation accuracy of LBHJAE was better than that of IBJAE (see Table V and Fig. 7). Note that when the distal part was 40% occluded, the performance of IBJAE was significantly reduced. However, the proposed LBHJAE mitigated the performance degradation by more than 53% with the help of KBJAE. In different sheath configurations, the estimation accuracy of KBJAE decreased with the increasing curvature angle of the sheath. Nevertheless, the proposed LBHJAE showed a performance improvement of about 47% over KBJAE alone (see Table VI) when the sheath was most bent. Note that when the tool was obscured and the sheath curvature was changed (see Table VII, occlusion (OC), sheath configuration (SC), Distal part (DP)). The proposed LBHJAE showed the best performance among the three methods.

When distal part of the instrument was covered about 40%, the performance of IBJAE was the worst. This is because the features

TABLE VI
ESTIMATION RESULTS IN DIFFERENT SHEATH CONFIGURATIONS

		Different sheath configurations			
Case		*0 °*	*90 °*	*180 °*	*270 °*
RMSE (°)	*KBJAE*	*2.37±0.27*	*4.20±0.68*	*6.07±1.03*	*6.81±3.97*
	IBJAE	*2.99±0.27*	*2.97±0.54*	***3.06±0.42***	***2.58±1.54***
	LBHJAE	***2.31±0.33***	***2.75±0.92***	*3.66±0.91*	*3.56±1.81*

TABLE VII
ESTIMATION RESULTS WITH BOTH OCCLUSION AND SHEATH CONFIGURATION CHANGES

	OC, SC	*40%, 270°*	*40% (DP), 180°*	*40% (DP), 270°*
RMSE (°)	*KBJAE*	*7.15±1.18*	*5.76±0.29*	*7.46±1.64*
	IBJAE	*9.15±1.42*	*9.675±0.7*	*8.61±1.46*
	LBHJAE	***6.85±1.08***	***5.755±0.66***	***5.97±0.99***

extracted by SCNN, determining the joint angle, are likely to be concentrated at the distal part. This is expected because the 2D appearance of the tool images with different bending angles are significantly different in the distal part. As the sheath curvature angle increases, hysteresis size also increases. Because KBJAE is not an adaptive method, its performance is degraded according to the increasing sheath curvature. When neither performs well, the proposed method can slightly improve the performance through stable and fast feedback using a Kalman filter.

B. Evaluation of Hysteresis Reduction Performance With the Proposed Compensator Using LBHJAE

1) Evaluation of Hysteresis Reduction Performance of LBHJAE in Surgical Instrument With Obscured Part: The purpose of this experiment was to evaluate the hysteresis reduction performance of the compensator with LBHJAE for a partially obscured surgical instrument.

The same conditions as the previous experiment were applied for the occlusion. A sinusoidal signal ($25\sin(t) + 25$, 0.159 Hz) was given as an input, and five repeating trajectories were given three times as a single signal. As an evaluation measurement, the RMS deviation between the desired angle and the actual angle measured from the Aurora sensor was used. In addition, the maximum hysteresis size, regarded as the peak-to-peak error between the desired input and measured output, was also considered.

The results are summarized in Table VIII and illustrated in Fig. 8. The results indicate that the accuracy of LBHJAE was better than that of IBJAE. Note that when the distal part of the surgical instrument was obscured 40%, the RMSE of IBJAE was the worst. On the other hand, the proposed LBHJAE improved the hysteresis reduction performance by more than 40% when the distal part of the instrument is occluded by 40%. Moreover, although this was inferior to KBJAE in some cases, the compensator with LBHJAE reduce hysteresis by about 47% compared to before the compensator was applied.

2) Evaluation of Hysteresis Reduction Performance of Compensator With LBHJAE in Various Sheath Shapes: The hysteresis reduction performance of the compensator using LBHJAE

TABLE VIII
HYSTERESIS REDUCTION RESULTS WITH AN OBSCURED PART

Case		Percentage of an obscured part			
		0%	20%	40%	40% (distal part)
RMSE (°)	None	7.84±2.23			
	KBJAE	2.48±0.7	**1.71±0.1**	**2.3±0.2**	**2.27±0.3**
	IBJAE	3.28±0.4	3.05±0.3	4.79±0.7	7.00±0.9
	LBHJAE	**2.08±0.5**	2.38±0.4	2.99±0.2	4.16±1.4
Maximum hysteresis size (°)	None	9.23±0.73			
	KBJAE	6.58±1.6	**4.52±0.5**	**4.49±0.6**	**3.14±1.1**
	IBJAE	5.17±0.9	6.25±1.3	7.44±0.2	15.3±3.9
	LBHJAE	**4.39±1.0**	5.14±1.4	6.29±0.9	7.84±1.0

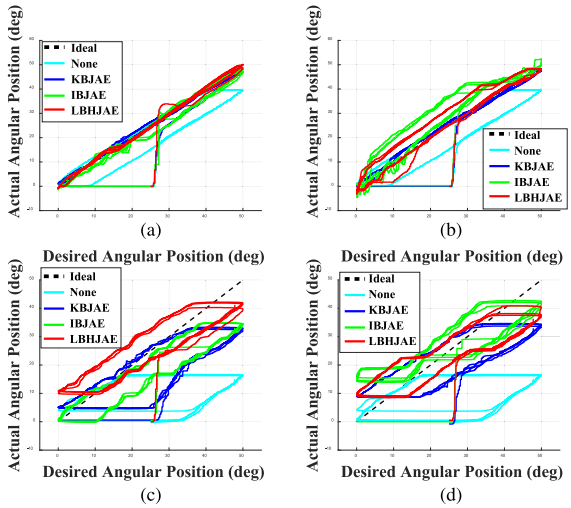

Fig. 8. Results of hysteresis reduction. (a) No occlusion and sheath configuration 0°. (b) 40% occlusion and sheath configuration 0°. (c) No occlusion and sheath configuration 270°. (d) 40% occlusion and sheath configuration 270°. (Ideal: black, None: cyan, KBJAE: blue, IBJAE: green, LBHJAE: red).

TABLE IX
HYSTERESIS REDUCTION RESULT IN DIFFERENT SHEATH CONFIGURATIONS

Case		Different sheath configurations			
		0 °	90 °	180 °	270 °
RMSE (°)	None	7.84±2.2	9.95±1.9	16.6±3.7	21.9±1.2
	KBJAE	2.48±0.7	5.09±1.7	9.27±2.9	12.8±1.8
	IBJAE	3.28±0.4	4.12±3.6	**5.96±0.2**	**8.1±1.8**
	LBHJAE	**2.08±0.5**	**3.66±0.1**	6.5±0.6	9.2±0.37
Maximum hysteresis size (°)	None	9.23±0.7	15.1±0.7	18.3±0.3	18.4±1.5
	KBJAE	6.58±1.6	**6.88±0.4**	11.9±0.1	17.6±2.0
	IBJAE	5.17±0.9	11.5±0.6	11.3±0.4	**11.2±3.0**
	LBHJAE	**4.39±1.0**	7.3±0.9	**8.19±0.9**	12.4±1.5

was compared to that of the compensator using IBJAE and KBJAE in various sheath configurations.

Four different sheath configurations were used as shown in Fig. 6(c). The input signal and evaluation criteria were the same as in the previous experiment.

The summary of the results is shown in Table IX and illustrated in Fig. 8. LBHJAE brought a 30% performance improvement over KBJAE only when the sheath configuration was deformed. In addition, although the performance of LBHJAE was lower than that of IBJAE in some cases, the compensator with LBHJAE reduced hysteresis by about 63% on average

TABLE X
HYSTERESIS REDUCTION RESULTS WITH BOTH OCCLUSION AND SHEATH CURVATURE CHANGES

	OC, SC	40%, 270°	40% (DP), 180°	40% (DP), 270°
RMSE (°)	KBJAE	13.02±1.77	9.79±0.87	12.07±0.78
	IBJAE	9.75±1.11	10.36±2.44	10.33±1.49
	LBHJAE	**9.09±0.82**	**7.09±0.45**	**9.32±0.47**

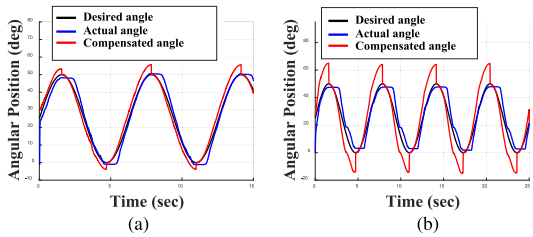

Fig. 9. Distinction between desired angle and compensated angle. (a) sheath configuration 0°. (b) sheath configuration 0°. (Actual: black, Desired angle: blue, Compensated angle: red).

compared to before the compensator was applied. Note that when the tool was obscured and the sheath curvature was also deformed, the proposed LBHJAE showed the best performance among the three methods (see Table X, occlusion (OC), sheath configuration (SC), Distal part (DP)).

IV. DISCUSSIONS

The results showed that the proposed LBHJAE was effective in estimating the joint angle as well as reducing hysteresis of the surgical instrument in both when the tool was occluded and when the sheath configuration was deformed. As shown in Fig. 9, the compensator provides the compensated angle using LBHJAE, which reduces hysteresis.

However, the proposed LBHJAE did not show the best performance in all situations. This is because, unlike the proposed method, KBJAE is not affected by occlusion and IBJAE is not influenced by deformed sheath configurations. Nevertheless, in real life, both occlusion and sheath configuration deformation can happen in combination. Therefore, it is appropriate to use the hybrid method, which prevents extreme performance loss, rather than use one method. To improve the performance, parameters R_1 and R_2 have to be updated online. We will refer to the adaptive adjustment of the noise covariance method [23] in our future work.

In addition, the following requirements should be additionally fulfilled for considering actual surgical operation. Firstly, the input signal from the master device is non-periodic, so it should be re-trained and re-evaluated with the signals acquired from the master. Secondly, hysteresis can be changed by the type of tool, manufacturing and assembly errors, wire slack, elongation, deterioration, the load on the tool, and even different sheath configurations. This may degrade the performance of KBJAE and LBHJAE. To solve this problem, the adaptive model with online estimation parameters should be applied. Li *et al.* showed that the method using wire force information could predict the current sheath configuration state [24]. Do *et al.* suggested the

adaptive controller for reducing hysteresis in the TSM using position feedback [25]. We expect that these can be useful in making a robust compensator regardless of changing hysteresis characteristics. Thirdly, the performance of IBJAE may be reduced in actual operation due to varying illumination, which can significantly degrade the performance of the current region-based segmentation method. To overcome this issue, we will use a more robust real-time image segmentation algorithm, such as a deep learning-based method in our future work. Fourthly, IBJAE must be re-trained and implemented taking account of the impact on additional DOFs. We will construct the database using a real surgery robot for training the deep network in expanding DOFs of the surgical instrument. Lastly, the evaluation should be carried out in a more complex and realistic environment, considering realistic motion, more complex phantom scenes, and the interaction between tools and phantoms.

We also have additional suggestions for making an effective compensator that noted through the experiments. In the compensator, using an overly high gain parameter may compromise stability and precision. In this case, applying the feed-forward controller as well helps reduce the initial error without using high gain.

V. Conclusion and Further Works

This letter introduced a novel LBHJAE method and demonstrated its effectiveness in hysteresis reduction by applying it to the compensator in a flexible surgery robot. We showed that this proposed hybrid method estimates the joint angle and reduces hysteresis of the surgical instrument when the tool is partially occluded and when sheath configurations are changed. The flexible endoscopic surgery robot testbed was used for all experiments and showed that the proposed method can improve the hysteresis reduction performance of a surgical instrument in a real surgery robot system. As a result, we showed that the proposed method works in a complementary manner, providing the best performance in complex situations involving actual surgery. In addition, it can be extended to visual servo-systems, which use camera and kinematic information in other applications.

In future work, we will use more robust segmentation methods and investigate other kinematic representations for KBJAE to consider actual surgical environments.

References

[1] J. Kim *et al.* "Effects of flexible surgery robot on endoscopic procedure: Preliminary bench-top user test," in *Proc. 28th IEEE Int. Conf. Robot Human Interactive Commun. (RO-MAN)*, New Delhi, India, 2019, pp. 1–6, doi: 10.1109/RO-MAN46459.2019.8956333.

[2] D. B. Camarillo, C. F. Milne, C. R. Carlson, M. R. Zinn, and J. K. Salisbury, "Mechanics modeling of Tendon - driven continuum manipulators," *IEEE Trans. Robot.*, vol. 24, no. 6, pp. 1262–1273, Dec. 2008.

[3] R. Roy, L. Wang, and N. Simaan, "Modeling and estimation of friction, extension, and coupling effects in multi segment continuum robots," *IEEE/ASME Trans. Mechatronics*, vol. 22, no. 2, Apr. 2017, Art. no. 909920.

[4] T. N. Do, T. Tjahjowidodo, M. W. S. Lau, T. Yamamoto, and S. J. Phee, "Hysteresis modeling and position control of tendon-sheath mechanism in flexible endoscopic systems," *Mechatronics*, vol. 24, no. 1, pp. 12–22, 2014.

[5] W. Xu, J. Chen, H. Y. K. Lau, and H. Ren, "Data-driven methods towards learning the highly nonlinear inverse kinematics of tendon-driven surgical manipulators," *Int. J. Med. Robot.*, vol. 13, no. 3, 2017, doi: 10.1002/rcs.1774.

[6] R. A. Porto, F. Nageotte, P. Zanne, and M. de Mathelin, "Position control of medical cable-driven flexible instruments by combining machine learning and kinematic analysis?," in *Proc. IEEE Int. Conf. Robot. Autom.*, 2019, pp. 7913–7919.

[7] Y. Liang, Z. Du, W. Wang, and L. Sun, "A novel position compensation scheme for cable-pulley mechanisms used in laparoscopic surgical robots," *Sensors*, vol. 17, 2017, Art. no. 2257.

[8] T. Reichl, J. Gardiazabal, and N. Navab, "Electromagnetic servoing - a new tracking paradigm," *IEEE Trans. Med. Imag.*, vol. 32, no. 8, pp. 1526–1535, Aug. 2013.

[9] P. Cabras, F. Nageotte, P. Zanne, and C. Doignon, "An adaptive and fully automatic method for estimating the 3D position of bendable instruments using endoscopic images," *Int. J. Med. Robot. Comput. Assist. Surg.*, vol. 13, Dec. 2017, Art. no. e1812, doi: 10.1002/rcs.1812.

[10] A. Reiter, P. K. Allen, and T. Zhao, "Appearance learning for 3D tracking of robotic surgical tools," *Int. J. Robot. Res.*, vol. 33, no. 2, 2014, Art. no. 342356.

[11] A. Reiter, R. E. Goldman, A. Bajo, K. Iliopoulos, N. Simaan, and P. K. Allen, "A learning algorithm for visual pose estimation of continuum robots," *IEEE Int. Conf. Intell. Robots Syst.*, 2011, pp. 2390–2396.

[12] R. Reilink, S. Stramigioli, and S. Misra, "Image-based hysteresis reduction for the control of flexible endoscopic instruments," *Mechatronics*, vol. 23, pp. 652–658, 2013.

[13] D. Baek, J.-H. Seo, J. Kim, and D.-S. Kwon, "Image-based hysteresis compensator for a flexible endoscopic surgery robot," in *Proc. 16th Int. Conf. Ubiquitous Robots*, 2019, pp. 299–305.

[14] H. Kim, M. Hwang, J. Kim, J. M. You, C.-S. Lim, and D.-S. Kwon, "Effect of backlash hysteresis of surgical tool bending joints on task performance in teleoperated flexible endoscopic robot," *Int. J. Med. Robot. Comput. Assisted Surgery*, vol. 16, 2020, Art. no. e2047, doi: 10.1002/rcs.2047.

[15] J. Bromley *et al.*, "Signature verification using a siamese time delay neural network," *Int. J. Pattern Recognit. Artif. Intell.*, vol. 7, no. 4, pp. 669–688, 1993.

[16] G. Bradski and A. Kaehler, *Learning OpenCV: Comput. Vision with the OpenCV Library*. Sebastopol, CA, USA: O'Reilly Media, 2008.

[17] S. Soni *et al.*, "Kinematic and dynamic analysis of a surgical tool manipulator towards robotic surgery," in *Proc. 1st Int.,16th Nat. Conf. Mach. Mechanisms (iNaCoMM),*, IIT, Roorkee, India, 2013, pp. 987–991.

[18] D. Kingma and J. Ba, "Adam: A method for stochastic optimization," in *Proc. Int. Conf. Learn. Representations*, 2015, *arXiv:1412.6980*.

[19] X. Glorot and Y. Bengio, "Understanding the difficulty of training deep feedforward neural networks," in *Proc 13th Int. Conf. Artif. Intell. Statist.*, 2010, pp. 249–256.

[20] F. Ikhouane and J. Rodellar, *Systems With Hysteresis: Analysis: Identification And Control Using The Bouc Wen Model*. Hoboken, NJ, USA: Wiley, 2007.

[21] K. He, X. Zhang, S. Ren, and J. Sun, "Delving deep into rectifiers: Surpassing human-level performance on imagenet classification," 2015, *arXiv:1502.01852*.

[22] N Shivashankarappa, S. Adiga, R. A. Avinash, and H. R. Janardhan, "Kalman filter based multiple sensor data fusion in systems with time delayed state,", in *Proc. 3rd Int. Conf. Signal Process. Integr. Networks*, 2016, pp. 375–382.

[23] S. Akhlaghi, N. Zhou, and Z. Huang, "Adaptive adjustment of noise covariance in Kalman filter for dynamic state estimation," 2017, *arXiv:1702.00884*.

[24] X. Li, L. Cao, A. M. H. Tiong, P. T. Phan, and S. J. Phee, "Distal-end force prediction of tendon-sheath mechanisms for flexible endoscopic surgical robots using deep learning," *Mech. Mach. Theory*, vol. 134, pp. 323–337, 2019.

[25] T. N. Do, T. Tjahjowidodo, M. W. S. Lau, and S. J. Phee, "Adaptive control for enhancing tracking performances of flexible tendonsheath mechanism in natural orifice transluminal endoscopic surgery (notes)," *Mechatronics*, vol. 16, no. 2, pp. 161–188, 2015.

[26] J. H. Seo and D. S. Kwon, "Learning 3D local surface descriptor for point cloud images of objects in the real-world," *Robot. Auton. Syst.*, vol. 116, pp. 64–79, 2019.